frontiers in Marine Science

ORIGINAL RESEARCH
published: 15 March 2021
doi: 10.3389/fmars.2021.647394

Interplay Between Nanoplastics and the Immune System of the Mediterranean Sea Urchin *Paracentrotus lividus*

Carola Murano[1,2], Elisa Bergami[1], Giulia Liberatori[1], Anna Palumbo[2] and Ilaria Corsi[1]*

[1] Department of Physical, Earth and Environmental Sciences, University of Siena, Siena, Italy, [2] Department of Biology and Evolution of Marine Organisms, Stazione Zoologica Anton Dohrn, Naples, Italy

The present study highlights for the first time the interplay between model nanoplastics, such as the carboxyl-modified polystyrene nanoparticles (PS-COOH, 60 nm) NPs and the coelomocytes of the sea urchin *Paracentrotus lividus,* a benthic grazer widely distributed in Mediterranean coastal area, upon acute *in vitro* exposure (4 h) (5 and 25 $\mu g\ mL^{-1}$). Insight into PS-COOH trafficking (uptake and clearance) and effects on immune cell functions (i.e., cell viability, lysosomal membrane stability, and phagocytosis) are provided. Dynamic Light Scattering analysis reveals that PS NP suspensions in CF undergo a quick agglomeration, more pronounced for PS-COOH (608.3 ± 43 nm) compared to PS-NH_2 (329.2 ± 5 nm). However, both PS NPs are still found as nano-scale agglomerates in CF after 4 h of exposure, as shown by the polydispersity index > 0.3 associated with the presence of different PS NP size populations in the CF. The observed changes in ζ-potential upon suspension in CF (–11.1 ± 3 mV and –12.1 ± 4 mV for PS-COOH and PS-NH_2, respectively) confirm the formation of a bio-corona on both PS NPs. Optical fluorescence microscopy and fluorimetric analyses using fluorescently labeled PS-COOH (60 nm) reveal a fast uptake of PS-COOH primarily by phagocytes within 1 h of exposure. Upon transfer to PS NP-free CF, a significant decrease in fluorescence signal is observed, suggesting a fast cell clearance. No effect on cell viability is observed after 4 h of exposure to PS-COOH, however a significant decrease in lysosomal membrane stability (23.7 ± 4.8%) and phagocytic capacity (63.43 ± 3.4%) is observed at the highest concentration tested. Similarly, a significant reduction in cell viability, lysosomal membrane stability and phagocytosis is found upon exposure to PS-NH_2 (25 $\mu g\ mL^{-1}$), which confirms the important role of surface charges in triggering immunotoxicity. Overall, our results show that, although being quickly internalized, PS-COOH can be easily eliminated by the coelomocytes but may still be able to trigger an immune response upon long-term exposure scenarios. Taking into account that sediments along Mediterranean coasts are a sink for micro- and nanoplastics, the latter can reach concentrations able to exceed toxicity-thresholds for marine benthic species.

Keywords: sea urchin, nanoplastics, polystyrene, surface charge, immune cells, Mediterranean Sea

OPEN ACCESS

Edited by:
Nunziacarla Spanò, University of Messina, Italy

Reviewed by:
L. Courtney Smith, George Washington University, United States
Manu Soto, University of the Basque Country, Spain

****Correspondence:***
Carola Murano
carola.murano@student.unisi.it;
carola.murano@szn.it

Specialty section:
This article was submitted to Marine Pollution, a section of the journal Frontiers in Marine Science

Received: *29 December 2020*
Accepted: *22 February 2021*
Published: *15 March 2021*

Citation:
Murano C, Bergami E, Liberatori G, Palumbo A and Corsi I (2021) Interplay Between Nanoplastics and the Immune System of the Mediterranean Sea Urchin Paracentrotus lividus. Front. Mar. Sci. 8:647394. doi: 10.3389/fmars.2021.647394

INTRODUCTION

Being a semi-enclosed and convective basin, the Mediterranean Sea is a high plastic accumulation region, from where plastic debris can hardly elude (Cózar et al., 2015; Suaria et al., 2016; Macias et al., 2019). One of the latest basin-scale surveys estimated that 11.5 million of plastic pieces are floating over the entire Mediterranean region (Lambert et al., 2020). Through weathering, these plastics undergo chemical, physical and biological transformations, breaking down into microplastics (MPs, size < 1 mm) and nanoplastics (size < 1 μm) (Andrady, 2017; Hartmann et al., 2019). Such physico-chemical changes dictate both horizontal and vertical transport of plastic pieces of different size, which eventually sink to the seafloor, where they may significantly affect benthic communities (Courtene-Jones et al., 2017; Kane et al., 2020). Estimates of marine litter density in the seafloor of the Mediterranean Sea range from 0.25 to 30 items 100 m^{-2} with macroplastics representing up to 98% of the waste (Angiolillo et al., 2015; Macic et al., 2017; Consoli et al., 2018). In Mediterranean coastal sediments, MPs show a heterogeneous distribution, with abundances between 480 ± 9 and 2052 ± 746 MPs kg^{-1} of sediment (Alomar et al., 2016; Abidli et al., 2018; Simon-Sánchez et al., 2019). Spatial risk assessment studies highlighted that marine organisms living along the Mediterranean coasts are at higher risk of ingesting plastics, especially those with low motility and/or small home range, compared to open-sea species (Compa et al., 2019). However, despite the growing concern related to MPs presence in coastal seafloor, only few studies investigated MP ingestion in Mediterranean benthic species belonging to different phyla (i.e., Mollusca and Chordata) (Abidli et al., 2019; Vered et al., 2019). Avio et al. (2017) found synthetic microfibers in benthic organisms as the most abundant MPs, with a polymeric composition of polyethylene, polystyrene (PS) and nylon films. Nanoplastic contamination in Mediterranean marine ecosystems is still unknown, although a first study from Schirinzi et al. (2019) reported traces of nano-sized PS, in the range of 1.08 – 136.7 ng L^{-1} in estuarine and surface waters of the West Mediterranean Sea. Such findings raise concern due to the unique nanoscale properties of nanoplastics (i.e., high surface-volume ratio associated with remarkable biological, chemical and physical reactivity) that allow them to interact with the cellular machinery (Hewitt et al., 2020). As a result of the weathering process of plastic debris, once released in sea water (e.g., changes in crystallinity and surface oxidation), nanoplastics are expected to acquire oxygenated moieties, such as carboxylic groups (–COOH) and thus a negative surface charge (Fotopoulou and Karapanagioti, 2012; Gigault et al., 2016; Andrady, 2017). Therefore, the resulting behavior of nanoplastics in dynamic and stochastic systems, such as in seawater and in biological milieus, depends on nano-specific properties (e.g., surface charge, size, chemical composition, and functionalization) and those of the receiving environment (e.g., pH, ionic strength, natural organic matter content, and hydrodynamic conditions) (Corsi et al., 2020). The combination of these conditions defines nanoplastic ecological and ecotoxicological outcomes (Lowry et al., 2012; Mattsson et al., 2018). Specifically, functionalization and surface charge are responsible for the interfacial dynamics and thus the interactions with living systems (Corsi et al., 2020 and references within). In recent years, laboratory studies on nanoplastic impact assessment in marine species have investigated the effects of PS nanoparticles (PS NPs) as a proxy for nanoplastics. The most commonly tested ones are carboxyl-functionalized (–COOH) and amino-functionalized ($–NH_2$) PS NPs that exhibit a negative and positive surface charge, respectively. While PS-NH_2 display a striking toxicity in many marine models, leading to physiological alterations (Bergami et al., 2016, 2017; Varó et al., 2019), oxidative damage (Feng et al., 2019) and developmental impairments (Della Torre et al., 2014; Pinsino et al., 2017; Tallec et al., 2019; Eliso et al., 2020), the negatively charged counterpart (PS-COOH) is generally less harmful (Bergami et al., 2017; Manfra et al., 2017; Eliso et al., 2020). At first, the PS NP-biological interactions occur through the external surfaces of exposed organisms with potential routes that include ingestion, passage through gills, adsorption on body skin (Lead et al., 2018). At the cellular level, an interplay between PS NP surface charges and proteins and other biomolecules adsorbed onto NP surface has been elucidated, mainly focusing on the formation of the protein-corona, which is considered the bridge at the bio-nano interface (Canesi and Corsi, 2016; Canesi et al., 2016; Grassi et al., 2019). Grassi et al. (2019) identified the hard protein corona on surface charged PS NPs upon incubation in sea urchin CF. The authors showed that such bio-corona was dominated by the toposome precursor protein (TPP), a modified iron-less Ca^{2+} binding transferrin known as a biotic and environmental stress target (Castellano et al., 2018). This latest study has been conducted on the Mediterranean Sea urchin *Paracentrotus lividus*, a key species in the organization of benthic communities across Mediterranean coastal areas, controlling shallow macroalgal assemblages either as opportunistic generalist herbivore or as prey for various taxa (Barnes et al., 2002; Boudouresque and Verlaque, 2020). Thanks to its grazing activity, *P. lividus* has been identified as a bioeroder of plastic items, able to generate 92 ± 34 MPs over a 10 days period (Porter et al., 2019). Plastic ingestion has been reported in sea urchins collected along the coastal areas of northern China (Feng et al., 2020) as in other echinoderms such as holothurians and sand dollars (Graham and Thompson, 2009; Taylor et al., 2016; Plee and Pomory, 2020). However, to date no data are available on the presence of plastic debris in wild specimens of the sea urchin *P. lividus* in the Mediterranean Sea. The findings of our previous laboratory based research showed PS MPs (10–45 μm, 72 h) internalization and distribution in *P. lividus* organs (gonads, digestive, and water vascular systems), together with changes in the total number of immune cells (coelomocytes), and an increase in reactive nitrogen species (RNS) and ROS (Murano et al., 2020). Sea urchins show a distinctive immune system governed by coelomocytes, which are considered prominent biosensors for environmental monitoring (Pinsino and Matranga, 2015) and for studying environmental and anthropogenic challenges, such as ocean acidification, disused industrial activities, plastic pollution and engineered NPs (Falugi et al., 2012; Della Torre et al., 2014; Pinsino et al., 2015; Marques-Santos et al., 2018; Migliaccio et al., 2019; Alijagic et al., 2020; Milito et al., 2020; Murano et al., 2020). Recent investigations addressed the immunotoxicity of

positively charged PS–NH_2 on sea urchin coelomocytes, with apoptotic-like nuclear alterations, reduction in cell viability and destabilization of the lysosomal membranes (Marques-Santos et al., 2018). Although negatively charged nanoplastics are likely the most common ones found in marine waters, their toxicity toward marine benthic species has been overlooked. The aim of the present study is to investigate the interplay between negatively charged PS-COOH (60 nm), as a proxy for natural occurring nanoplastics, and *P. lividus* coelomocytes to unravel bio-nano interactions at cellular level and predict ecological damages. Positively charged PS-NH_2 (50 nm) at 25 $\mu g\ mL^{-1}$ have been tested as a surface charge counterpart. Following short-term exposure (4 h), the results obtained revealed a low acute toxicity of PS-COOH in comparison with PS-NH_2, as well as a fast uptake of PS-COOH by phagocytes and their sequestration into lysosomal compartments.

MATERIALS AND METHODS

Polystyrene Nanoparticles and Physico-Chemical Characterization

Unlabeled (60 nm, FC02N) and yellow-green fluorescently labeled carboxyl-modified PS NPs (PS-COOH, 60 nm, PC02N) (480/520 ex/em) as well as un-labeled amino-modified PS NPs (PS-NH_2, 50 nm, PA02N) were purchased from Bangs Laboratories Inc., Fishers, IN. Un-labeled PS-NH_2 and PS-COOH were used for *in vitro* exposure, while fluorescently labeled PS-COOH were used only for uptake and translocation experiments. Details about PS NP stock composition, labeling and surfactants/stabilizers content are reported in the **Supplementary Material**. With this regard, a rebuttal to the study of Pikuda et al. (2019) regarding the presence of stabilizers in PS NP stocks used in the present and our previous studies (Della Torre et al., 2014; Bergami et al., 2016, 2017; Pinsino et al., 2017) is also provided in the **Supplementary Material**. PS NPs stocks were briefly sonicated (bath sonicator CEIA CP316, at 600 W, 40 kHz, 3 min) and working suspensions (10 mg mL^{-1}) made in 0.22 μm milli-Q Water (mQW). In order to investigate PS NP behavior under the experimental conditions, hydrodynamic diameter (*Z*-average, nm) and polydispersity index (PdI, dimensionless) were determined by Dynamic Light Scattering (DLS), while ζ-potential (mV) was determined by electrophoretic mobility (EM), using a Zetasizer Nano ZS90 (Malvern Instruments). PS NP suspensions (25 mg mL^{-1}) were prepared in mQW and in immune cell exposure media (CF) and measurements carried out at 0 h and after 4 h at a constant temperature of 18°C.

Sea Urchin Collection and Immune Cell Culture

Fifty adult specimens of *P. lividus* were collected from the Tuscany coasts (42°26′10.99″N, 11°09′13.74″E, Italy), in an area not privately owned nor protected, according to the authorization of Marina Mercantile (DPR 1639/68, 09/19/1980, confirmed on 01/10/2000). Specimens were acclimated without feeding for 10 days in glass tanks filled with circulating natural seawater (NSW, 39 ± 1‰ salinity, pH 8, 18°C).

In vitro primary cultures of sea urchin coelomocytes were obtained following the protocol reported in Marques-Santos et al. (2018) and as previously described in Matranga et al. (2002). CF, used as exposure medium, was collected following the procedure reported in Marques-Santos et al. (2018) from a pool of eight individuals, displaying active movement and low number of red amebocytes with respect to the whole coelomocyte population. Soon after collection, CF was stored in Protein LoBind® Eppendorf tubes kept on ice prior to centrifugation at 600 × *g* for 20 min at 4°C. The supernatant was then sterile-filtered with 0.22 μm cellulose acetate syringe filters and stored at −80°C until use.

Sea urchin coelomocytes were obtained by using a 1 mL sterile syringe preloaded with CMFSW-EH anticoagulant solution (calcium and magnesium free seawater with EDTA and HEPES) at a ratio of 1:1 to prevent clotting (NaCl 460 mM; KCl 10.7 mM; EDTA 70 mM; Hepes 20 mM; Na_2SO_4 7 mM; $NaHCO_3$ 2.4 mM, pH 7.4) following the protocol of Smith et al. (2019). Cell suspension was obtained after CF centrifugation at 600 × *g* for 5 min at 4°C and suspension in 0.22 μm filtered CF, obtained as described above.

The composition of the heterogeneous coelomocyte population (i.e., phagocytes, vibratile cells, white and red amoebocytes), based on Pinsino and Matranga (2015) was evaluated using Luna II Automated cell counter (Logos Biosystems Inc., see SI for instrument settings) and further confirmed under optical microscopy using FastRead® 102 chamber.

Coelomocytes suspensions in CF ($1{\cdot}10^6$ cells mL^{-1}) were exposed to un-labeled PS-COOH (5 and 25 $\mu g\ mL^{-1}$) and PS-NH_2 (25 $\mu g\ mL^{-1}$) in sterile 24 well plates (final volume of 1 mL) at 18°C in the dark. PS-NH_2 was used as a positively charged counterpart (25 $\mu g\ mL^{-1}$), based on previous findings from Marques-Santos et al. (2018). After 4 h incubation, cells were collected for viability, lysosomal membrane stability and phagocytosis assays. Each experiment was run 3 times. The tested concentrations of PS NPs for acute exposure were chosen according to our previous studies with sea urchin coelomocytes (Marques-Santos et al., 2018; Bergami et al., 2019). Here, the acute exposure conditions tested can be predictive of worst-case scenarios in Mediterranean coastal areas and crucial to improve our knowledge of the effects of PS NPs for environmental risk assessment purposes.

Cell Viability

The trypan blue exclusion test was performed following the protocol of Strober (2015). At each time-point (0 and 4 h), coelomocytes in CF were collected ($1{\cdot}10^6$ cells mL^{-1}), centrifuged at 600 × g for 10 min at 4°C and then incubated in trypan blue in PBS-1X (0.4%) for 4 min and examined after adhesion on glass slides under optical microscope (Olympus BX51, Tokyo, Japan). Percentage of viable cells in the whole coelomocyte population was calculated as the number of viable

cells *vs.* the number of total cells. For each experimental group, the assay was performed in triplicate and run three times.

Lysosomal Membrane Stability

Neutral red retention time (NRRT) assay (Lowe et al., 1995) was adapted to coelomocytes following the protocol described in Marques-Santos et al. (2018). The NRRT assay was carried out using the NR dye as a marker of phagosome acidification in phagocytes (Pinsino et al., 2015), but it also stains primary lysosomes of vibratile cells (Pinsino and Matranga, 2015), which were included in the assay. After 4 h of exposure to PS NPs, 200 μL of cell suspensions were placed on a glass coverslip (22 × 22 cm) and incubated for 1 h in a humid chamber at 18°C in the dark. Cells were then incubated for 30 min at 18°C with 200 μL of NR dye solution (final concentration of 40 μg mL^{-1} from a stock solution of 40 mg mL^{-1} NR in DMSO). The excess of the dye was removed using a buffer solution (20 mM Hepes; 436 mM NaCl; 53 mM $MgSO_4$; 12 mM KCl; 12 mM $CaCl_2$, pH 7.5) and coverslips placed on slide and sealed. Slides were checked every 15 min under an optical microscope (40X, Olympus BX51, Tokyo, Japan) and the percentage of cells showing loss of NR dye into the cytosol was counted. An average of 100 cells were scored at each time-point and end-point set when 50% of the cells showed signs of lysosomal leaking (cytosol becoming red and cells rounded shaped). The assay was run in triplicate and three times.

Phagocytosis

The phagocytosis assay was run as described in Bergami et al. (2019) and following the protocol by Borges et al. (2002) with slight modifications, as reported below. Before the assay, fresh suspensions of the yeast (*Saccharomyces cerevisiae*) in 0.22 μm filtered NSW were prepared and yeast cells counted using Luna II Automated cell counter (Logos Biosystems Inc., **Supplementary Figure S1**). The assay was run using coelomocytes collected after 4 h of exposure, placing 200 μL of cell suspension on a coverslip and incubating with yeast cells suspension for 1 h in a ratio 1:10 (phagocytes: yeast) in a humid chamber at 18°C in the dark. Coverslips were then washed with filtered NSW, fixed in ice-cold methanol for 20 min, air-dried and then stained with Giemsa (6%). A minimum of 100 cells per experimental group was observed under an optical microscope (Olympus BX51, Tokyo, Japan). Phagocytosis-related parameters were calculated on the phagocyte sub-population according to Borges et al. (2002): phagocytic capacity (PC,%) and phagocytic index (PI,%) as the number of phagocytes internalizing yeast on the total phagocytes and the number of yeast cells internalized related to the number of phagocytes containing the yeast, respectively.

Cellular Uptake of PS-COOH

In order to evaluate the uptake of PS-COOH in sea urchin phagocytes, yellow-green fluorescently labeled PS-COOH (Dragon green labeling ex/em 480/520) were used. The fluorophore of labeled PS-COOH was embedded within the polymer during synthesis (see **Supplementary Material** for further details), thus preventing any leaching of the dye during testing. However, as underlined by the most recent literature, the stability of PS NP fluorophore should also be proven prior to use to avoid artifacts when studying NP uptake and translocation by fluorescence imaging and confocal laser scanning microscopy (Catarino et al., 2019; Schür et al., 2019). Here we further confirmed the stability of PS-COOH fluorophore during the exposure study (4 h in CF) using the following protocol. Labeled PS-COOH (25 μg mL^{-1}) were suspended in CF and collected at time 0 and after 4 h, centrifuged using Microcon® (10 kDa) tubes at 7000 × *g* for 30 min at 18°C and the fluorescence signal measured using Tecan spectrophotofluorimeter (Infinite M1000 Pro). CF alone was also analyzed to determine the background auto-fluorescence (see **Supplementary Figure S2**).

For the uptake study, monolayers of coelomocytes in CF ($1{\cdot}10^6$ cells mL^{-1}) on a glass slide were exposed to fluorescently labeled PS-COOH (5 and 25 μg mL^{-1}) in the dark at 18°C in a humid chamber. At different time-points (0, 15, 30 min, 1 h, 4 h) cells were observed under an optical microscope (Olympus BX51, Tokyo, Japan) equipped with a fluorescence filter (488 λ_{ex}-510 λ_{em}). Quantitative measurements of the fluorescence signal were also performed using fluorimetry. Prior to analysis, the fluorescence intensity signal of fluorescently labeled PS-COOH suspensions in CF (without cells) was measured by using a multi-plate spectrofluorimeter (Victor 3 Perkin Elmer 1420 Multilabel Counter) in PS-COOH (5 and 25 μg mL^{-1}) incubated in CF for 4 h. Fluorescence (arbitrary units, a.u.) was calculated subtracting the auto-fluorescence of CF alone.

Coelomocytes suspensions in CF (300 μL) were then incubated with fluorescently labeled PS-COOH (5 and 25 μg mL^{-1}) following the same procedure described above. After 4 h, suspensions were centrifuged at 600 × *g* for 10 min at 4°C, washed twice in CF, tip-sonicated (30 s 100 w, 1 cycle) in an ice-cool bath at 4°C and centrifuged again at 13000 × *g* for 10 min at 4°C. The resulting supernatant was transferred in 96-well black plates and the fluorescence (a.u.) measured by a multi-plate spectrofluorimeter (Victor 3 Perkin Elmer 1420 Multilabel Counter). Cell suspensions of control groups (incubated in CF only) were processed alike. Each reading was run in triplicate. Fluorescence (a.u.) was calculated by subtracting the auto-fluorescence of the control group.

Confocal laser scanning microscopy was used to assess PS-COOH uptake by coelomocytes. Monolayers of coelomocytes suspensions in CF ($1{\cdot}10^6$ cells mL^{-1} on coverslips) were fixed in 4% paraformaldehyde (in PBS) for 1 h at room temperature, then washed three times with PBS and incubated with Hoechst 33342 dye (10 μg mL^{-1}) and Red Phalloidin- Alexa 555 dye (1:100 in PBS) for 30 min. Coverslips were then placed on glass slides and observed by a confocal laser scanning microscope (Leica TCS SP8X) and images analyzed by the LAS X Life Software and ImageJ Software (Wayne Rasband, Bethesda, MA, United States). A control group of unexposed cells (in CF only) was also processed and analyzed. All images were acquired using the same gain and pinhole aperture in order to assess the differences among the treatments, in terms of signal intensity at the same spatial resolution, and to avoid the saturation or photodamage effects of the fluorescence signal (Pawley, 2006).

A recovery experiment was also performed in order to estimate the clearance of PS-COOH from coelomocytes. Cell

suspensions in CF (300 μL) were exposed to fluorescently labeled PS-COOH for 1 h (5 and 25 μg mL^{-1}), as described above. Cells were then centrifuged at 600 × g for 10 min at 4°C, resuspended in CF (without NPs). After 3 h exposure to CF only, cells were washed in CF and processed for the fluorimetry analysis as described above.

Scanning and Transmission Electron Microscopy

Coelomocytes ($1{\cdot}10^6$ cells mL^{-1}) were exposed to CF only and to 25 μg mL^{-1} of fluorescently labeled PS-COOH for 4 h. Coelomocytes (50 μL) were then transferred to a filter Swinnex system® and fixed with 1% glutaraldehyde in 0.1 M cacodylate buffer in NSW (pH 7.5) at 4°C overnight and post-fixed with 1% osmium tetroxide in cacodylate buffer. Cells were washed three times in 0.1 M cacodylate buffer in NSW, dehydrated through an ethanol series (25, 50, 75, and 100%), and dried in a sputter coated with gold, using a Leica ACE200 vacuum coater (Leica Microsystems, Inc. Buffalo Grove, IL, United States). Observations were performed with a scanning electron microscope (SEM) JSM-6700F (JEOL USA, Inc. Peabody, MA, United States). For transmission electron microscopy (TEM) analysis, coelomocytes were transferred to an Eppendorf tube (2 mL) and fixed with 3% glutaraldehyde in 0.1 M cacodylate buffer in NSW (pH 7.5) at 4°C overnight. Samples were then post-fixed overnight at 4°C with 1% osmium tetroxide in cacodylate buffer. Cells were washed three times in cacodylate buffer and three times in distilled water, and embedded into 4% low-melt agarose. Samples were finally dehydrated through a graded ethanol series and embedded in epoxy resin (EPON 812). The ultrathin sections were performed with Leica Ultracut ultramicrotome, stained with uranyl-less (EMS Catalog #22409) and lead citrate solution and observed with a TEM LEO 912AB. All images were processed with ImageJ Software (Wayne Rasband, Bethesda, MA, United States).

Statistical Analysis

Statistical analyses were performed using GraphPad Prism version 7.00 for Windows. Distribution of the data set was evaluated using a Shapiro–Wilk test and transformed where suitable. Data obtained from the NRRT assay were analyzed by One-way analysis of variance ANOVA followed by Tukey's Post-test. Viability assay and phagocytic activity were analyzed by Kruskal–Wallis test followed by Dunn's post-test. All data were presented as mean ± SD and were considered statistically significant at p-value < 0.05.

RESULTS

Agglomeration of Polystyrene Nanoparticles in *P. lividus* Coelomic Fluid

DLS and EM are widely recognized as suitable tools for the physico-chemical characterization of nanoscale particles in nanoecotoxicology (Corsi et al., 2020). They have been used to assess behavior and stability of PS NPs (PS-COOH and PS-NH_2) colloidal suspensions under conditions of optimal dispersion in mQW and under more environmentally relevant experimental conditions, as those in sea urchin CF used for primary culture of coelomocytes. The DLS analysis revealed an optimal dispersion and stability of both PS NPs in mQW up to 4 h, with NP size-related parameters close to their nominal size (50–60 nm), as shown by Z-average and PdI values (**Figures 1A,B**). EM analysis confirmed PS NP surface charge in mQW and over time (0–4 h), as indicated by ζ-potential (mV) negative values for PS-COOH (from −57.4 ± 1.3 to −42.5 ± 3.7 mV) and positive ones for PS-NH_2 (from +39.7 ± 2.1 to +45.8 ± 0.7 mV) (**Figure 1**). A different behavior was observed for PS NPs in CF (i.e., the exposure medium), as indicated by the presence of large agglomerates (in the size range of 300–600 nm) shown by DLS analysis, even soon after the preparation of the suspension (at 0 h). PS-COOH suspensions in CF were characterized by a heterogeneous size distribution (PdI values > 0.5), forming large agglomerates with an average size of 600 nm at 0 and 4 h. Differently, PS-NH_2 suspensions presented two main peaks in the size distribution (PdI values > 0.3), corresponding to two size populations at approximately 80 and 500 nm, thus forming smaller agglomerates (average size of 330 nm) in CF and still stable up to 4 h. The EM analysis showed a general lower stability of PS NPs in CF compared to mQW. PS-COOH still maintained their negative surface charge over time (0–4 h) (from −11.1 ± 2.7 to −9.0 ± 1.2 mV), while PS-NH_2 acquired a new negative charge (from −12.1 ± 3.9 to −9.3 ± 2.1 mV) similar to the one of PS-COOH in CF.

Overall, DLS and EM analyses confirmed the nanoscale properties of either anionic and cationic functionalized PS NPs when suspended in mQW, with narrow size distributions centered in their hydrodynamic diameter and preserved their negative (PS-COOH) and positive (PS-NH_2) surface charge. Such features, indicating an optimal dispersion, were lost once PS NPs were suspended in sea urchin CF in which, regardless NP surface charges, they show an unstable multimodal size distribution mostly related to their known interplay with inorganic and organic molecules of the CF (Marques-Santos et al., 2018; Grassi et al., 2019).

Immunotoxicity Induced by PS NPs on *P. lividus* Coelomocytes

Coelomocytes are a heterogeneous group of circulating cells located in sea urchin CF, with a majority of phagocytes (>80%) and other cell sub-populations present in lower quantities, such as red and white amoebocytes (≈ 13%) and vibratile cells (≈ 7%) (Pinsino and Matranga, 2015). Since each cell sub-population has key functions in sea urchin innate immunity, the immune response toward external challenges can be first assessed through the count of coelomocyte sub-populations (Branco et al., 2013; Migliaccio et al., 2019). Total immune cells count showed no variations in coelomocyte sub-populations, represented by phagocytes, red amoebocytes, white amoebocytes and vibratile cells upon exposure to PS NPs. No significant differences in cell viability upon exposure to PS-COOH at both concentrations tested were observed compared to the control

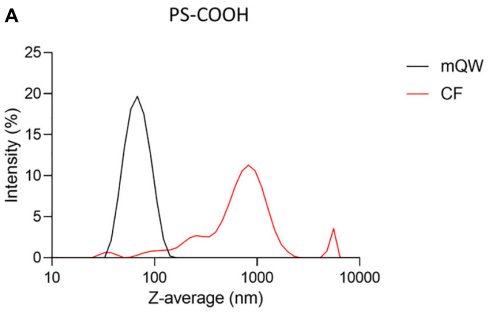

Medium	Time (h)	Z-average (nm)	PdI	ζ-potential (mV)
COOH-mQW	0	62.68 ± 1.20	0.124 ± 0.020	-57.4 ± 1.34
	4	56.67 ± 0.98	0.251 ± 0.013	-42.5±3.72
COOH-CF	0	608 ± 43	> 0.500	-11.1 ± 2.68
	4	647 ± 35	> 0.500	-9.0 ± 1.22

Medium	Time (h)	Z-average (nm)	PdI	ζ-potential (mV)
NH_2-mQW	0	50.37 ± 0.25	0.171 ± 0.026	+39.7 ± 2.10
	4	49.88 ± 0.78	0.196 ± 0.017	+45.8 ± 0.75
NH_2- CF	0	329 ± 5	> 0.300	-12.1 ± 3.94
	4	324 ± 17	> 0.300	- 9.32 ± 2.06

FIGURE 1 | Polystyrene nanoparticles behavior in exposure media. Particles size distribution and *Z*-average (nm), polydispersity index (PdI) and ζ-potential (mV) of unlabeled PS-COOH **(A)** and PS-NH_2 **(B)** in mQW and coelomic fluid (CF) at time 0 and 4 h. Data are referred to 25 μg mL^{-1} of PS NPs and reported as mean ± SD (*n* = 3).

group. Conversely, a significant decrease in cell viability after exposure to PS-NH_2 (25 μg mL^{-1}) was found (**Figure 2** and **Supplementary Figure S3-A**).

Lysosomal Membrane Stability Decrease at the Highest PS-COOH Concentration

Lysosomes are cellular organelles involved in different membrane-trafficking pathways, including endocytosis and phagocytosis of foreign particles. The NRRT assay used to assess lysosomal membrane stability is based on the ability of phagocytes to accumulate the NR dye inside their lysosomal compartments. Once lysosomal membranes are destabilized, the dye is then released inside the cytosol (Lowe et al., 1995). A significant increase in the percentage of destabilized lysosomes was observed in coelomocytes exposed to 25 μg mL^{-1} of PS-COOH and PS-NH_2 compared to the control group, already after 30 min of incubation with the NR dye (**Figure 3**). Differently, no differences in the percentage of destabilized lysosomes were observed in coelomocytes exposed at the lowest PS-COOH concentration (5 μg mL^{-1}), compared to the control group (in CF only). In general, the effects of PS NPs on the destabilization of the lysosomal membranes appeared to be limited, since no experimental group reached 50% of lysosomal destabilization after 60 min of exposure, which is commonly considered the toxicity end-point of this assay (ICES, 2010; Davies et al., 2012).

Phagocytosis Activity Is Concentration- and Surface Charge-Dependent

Sea urchin phagocytes have a primary role in innate immunity, allowing for clotting and internalization of foreign particles, cytolysis and secretion of humoral factors (reviewed in Smith et al., 2018). A change in the phagocytic activity of these cells, determined through the phagocytosis assay, indicates their ability to cope with a new immune challenge which may affect cell metabolism and viability. Results on PC and PI are shown in **Figure 4**. Phagocytes exposed to 25 μg mL^{-1} of PS-COOH and PS-NH_2 showed a significant decrease in PC compared to the control group (**Supplementary Figure S3-C**). The lowest concentration of PS-COOH led to a PC and a PI similar to the control group (**Supplementary Figure S3-C**). A significant decrease in PI was found only for coelomocytes exposed to PS-NH_2 (124.2 ± 14.3%) while no changes were found between those exposed to PS-COOH and the control group.

Overall, the results on *P. lividus* cell immune parameters in response to short-term exposure to PS NPs show differences according to PS NP surface charge (PS-COOH *vs.* PS-NH_2). Negatively charged PS-COOH did not affect cell viability but caused a destabilization of lysosomal membranes only at the highest concentration (25 μg mL^{-1}). Furthermore, PS-COOH provoked a reduction in PC, but did not affect the quality of the phagocytes, in terms of PI, as found instead for PS-NH_2.

Fast Uptake and Compartmentalization of PS-COOH in Phagocytes

The use of yellow-green fluorescently labeled PS-COOH allowed us to evaluate their uptake, translocation and clearance in the phagocytes, the most abundant coelomocyte sub-population of *P. lividus*, having a key role in innate immunity. Optical fluorescence images of coelomocytes exposed to PS-COOH at both concentrations (5 and 25 μg mL^{-1}) show NP uptake already

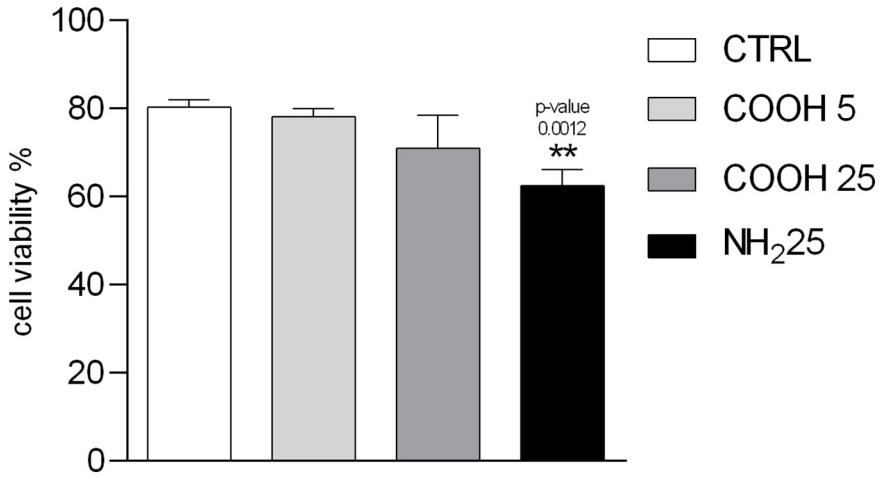

FIGURE 2 | Immune cell viability. Percentage of viable *P. lividus* coelomocytes *vs.* total number of cells screened after 4 h of exposure to CF (control), PS-COOH (5 and 25 μg mL^{-1}) and PS-NH$_2$ (25 μg mL^{-1}). Data are reported as mean ± SD (n = 9; Kruskal–Wallis test, Dunn's post-test, $p < 0.01$). ** Indicate significant differences with respect to the control group.

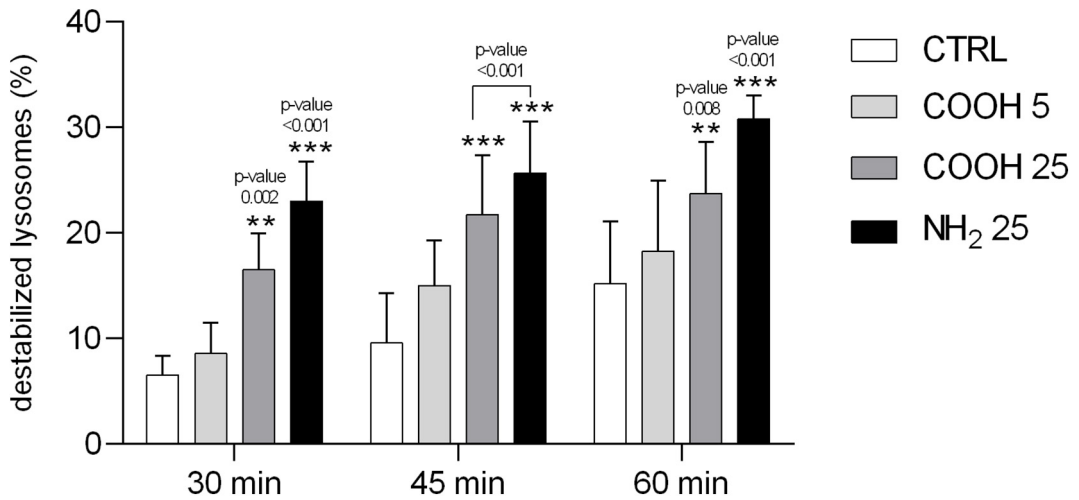

FIGURE 3 | Lysosomal membrane stability of sea urchin coelomocytes. Percentage of destabilized lysosomes scored in 100 *P. lividus* coelomocytes after 4 h of exposure to PS-COOH (5 and 25 μg mL^{-1}) and PS-NH$_2$ (25 μg mL^{-1}). Data are reported as mean ± SD (n = 6, One-way, Tukey's post-test, $^{**}p < 0.01$, $^{***}p < 0.001$). Asterisks indicate significant differences with respect to control and PS-COOH (5 μg mL^{-1}) exposure groups.

after 15 min and 30 min of exposure (**Supplementary Figure S4**). Fluorescence signal was still evident after 4 h and more evident on *P. lividus* phagocytes compared to the other cell populations (**Supplementary Figure S5**). The fluorescence intensity recorded in lysed phagocytes was significantly higher only in those exposed at the highest PS-COOH concentration (25 μg mL^{-1}) compared to the control group, while no changes were observed for those exposed to 5 μg mL^{-1} up to 4 h of exposure (**Figure 5**) (**Supplementary Figure S3-D**). The fluorescence intensity of cell lysates exposed to low and high concentrations of PS-COOH was in the ratio 1: 5 in line with the ratio of their nominal concentrations (5 and 25 μg mL^{-1}). Furthermore, the evidence that the intensity measured effectively represented only the internalized PS-COOH is given by the fact that the fluorescence intensity of the PS-COOH suspended in CF only is an order of magnitude higher with respect to the intensity of cell lysates (**Supplementary Figure S6**).

Confocal analysis confirmed the internalization of fluorescently labeled PS-COOH agglomerates inside lysosomes of phagocytes at both concentrations tested (5 and 25 μg mL^{-1}) and in a concentration dependent manner (**Figure 6**). PS-COOH were also found close to cell membranes where they could stimulate an inflammatory response. In particular, the images, obtained at the same gain and at the same pinhole, showed that the internalized particles were organized in circular structures recognizable as lysosomes (**Figure 6**). Moreover, confocal microscopy highlighted the presence of multinucleate coelomocytes as a result of cell fusion into a syncytium, a

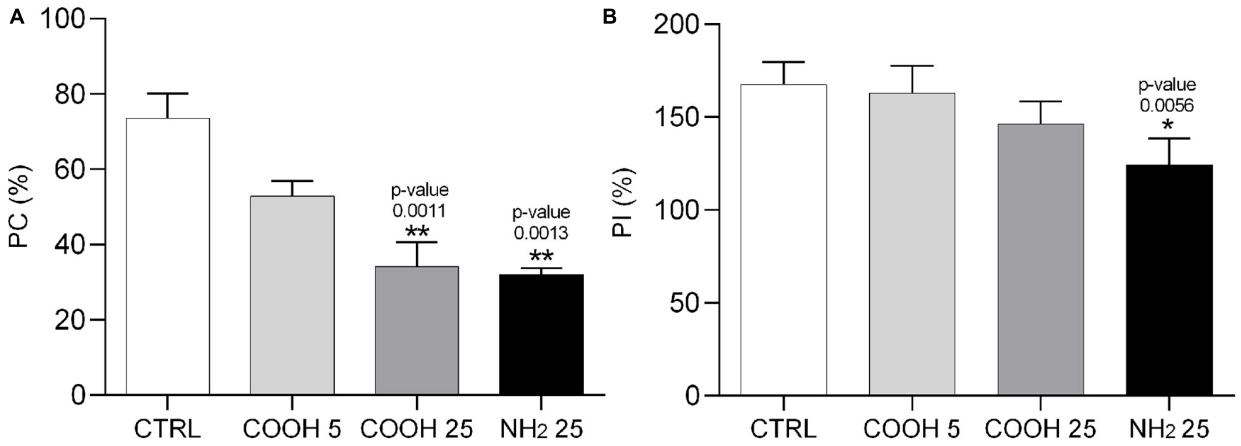

FIGURE 4 | Phagocytosis activity assay in sea urchin phagocytes. Phagocytic capacity (PC, %) **(A)** and phagocytic index (PI, %) **(B)** calculated on *P. lividus* phagocytes after 4 h of exposure to PS-COOH (5 and 25 μg mL^{-1}) and PS-NH$_2$ (25 μg mL^{-1}). Data are reported as mean ± SD (n = 9, Kruskal–Wallis test, Dunn's post-test, *$p < 0.05$, **$p < 0.01$). Asterisks indicate significant differences with respect to the control group.

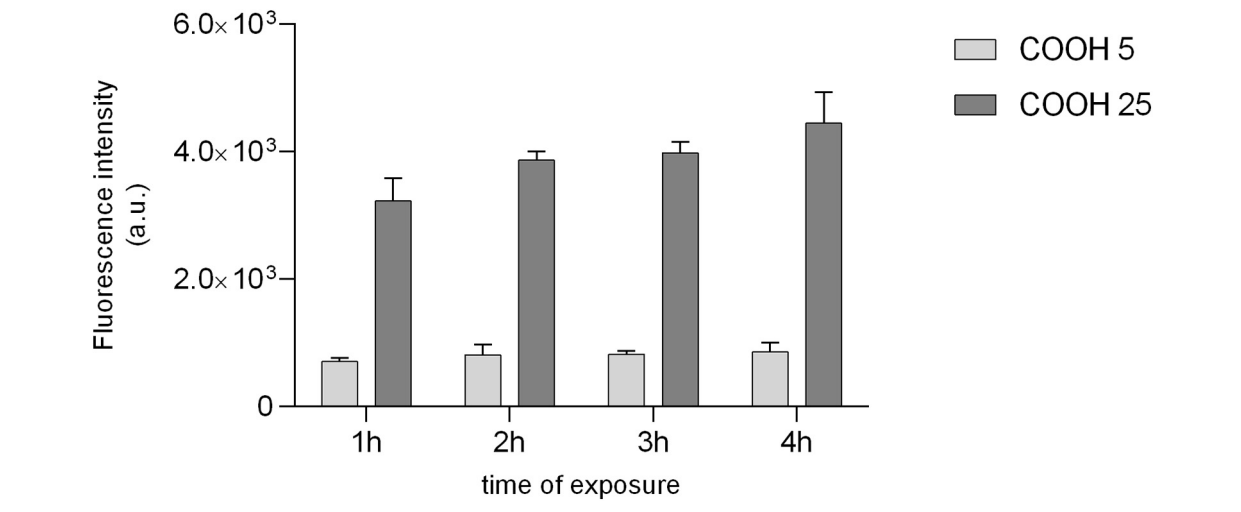

FIGURE 5 | Uptake of PS-COOH in sea urchin phagocytes. Fluorescence intensity (arbitrary units, a.u.) of immune cells exposed to fluorescently labeled PS-COOH (5 and 25 μg mL^{-1}) at 0 h and after 1, 2, 3, and 4 h of exposure. Bars represent mean ± SD (n = 3). Fluorescence intensity values are normalized to the auto-fluorescence signal of the control group (*P. lividus* cells exposed to CF only) at each time-point.

typical process in echinoderm phagocytes (Majeske et al., 2013; Pinsino and Matranga, 2015). Fluorescence measurements of coelomocytes lysates from the recovery experiment showed a significant lower intensity in the fluorescence signal with a reduction of over 50% after 3 h in CF compared to values recorded in cell lysate after 1 h of exposure at both PS-COOH concentrations (5 and 25 μg mL^{-1}) (**Figure 7**) (**Supplementary Figure S3-E**).

A fast uptake (<15 min) and a time-dependent internalization of the fluorescently labeled PS-COOH NPs in immune cells of sea urchin was shown at 25 μg mL^{-1}. PS-COOH were mostly internalized in lysosomes of coelomocytes but also localized as small agglomerates in the perinuclear area but apparently not inside the nucleus. On the other hand, based on fluorescence microscopy and quantitative fluorimetric analysis, ∼50% of PS-COOH seemed to be eliminated from the cells after 1 h of exposure, regardless of tested concentrations (5 and 25 μg mL^{-1}).

Changes in Coelomocytes Ultrastructural Properties

To assess the possibility that PS-COOH could modify coelomocyte ultrastructure, SEM and TEM analyses were performed. SEM images showed a regular and homogeneous surface morphology of the phagocytes of the control group, while a heterogeneous surface was found in PS NP-exposed cells, characterized by the presence of a biological adhesive matrix (flocculate-like structures) presumably resulting from the interaction between CF components and PS-COOH

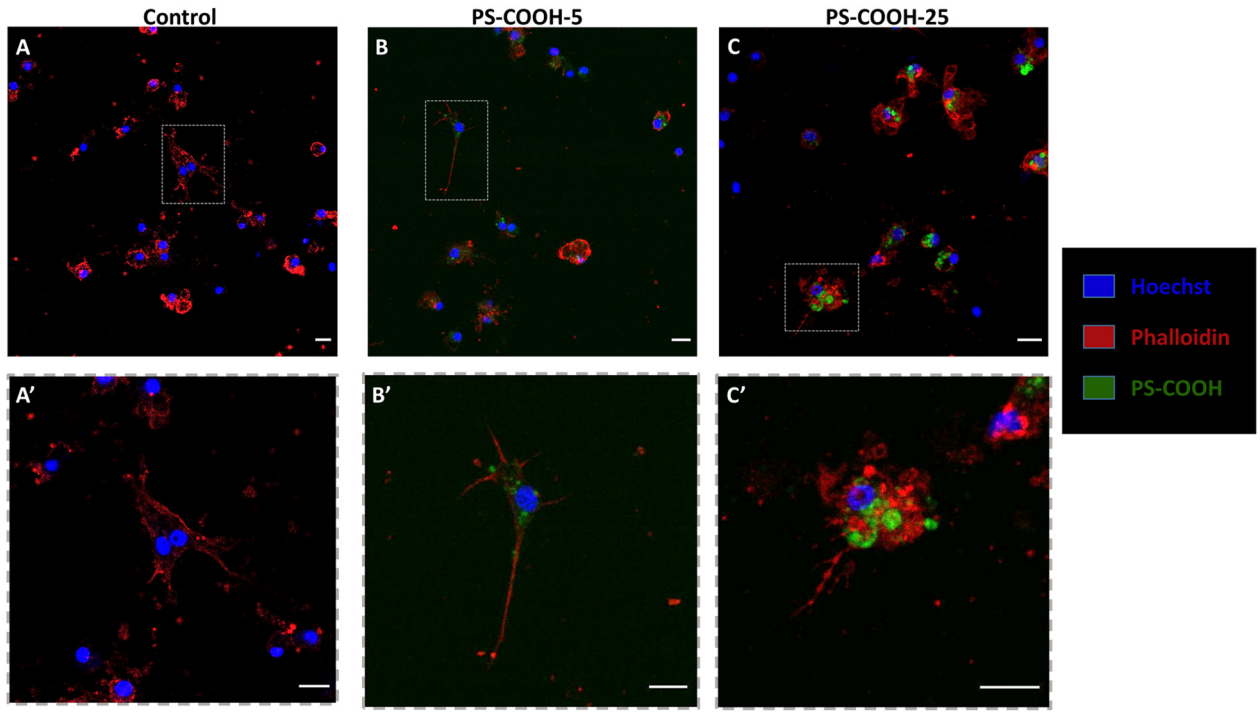

FIGURE 6 | PS-COOH disposition in sea urchin phagocytes by confocal microscopy. **(A)** Control phagocytes (exposed to CF only). **(B,C)** Internalization of fluorescent labeled PS-COOH (5 and 25 μg mL^{-1}) in phagocytes of sea urchin *P. lividus* upon 4 h of exposure (blue: nuclei, red: actin and green: PS-COOH). **(A',B',C')** Higher magnifications of the areas in the upper images are reported in the images at the bottom. Images were recorded with the same gain using a confocal microscope (Leica TCS SP8X). Scale bar: 10 μm.

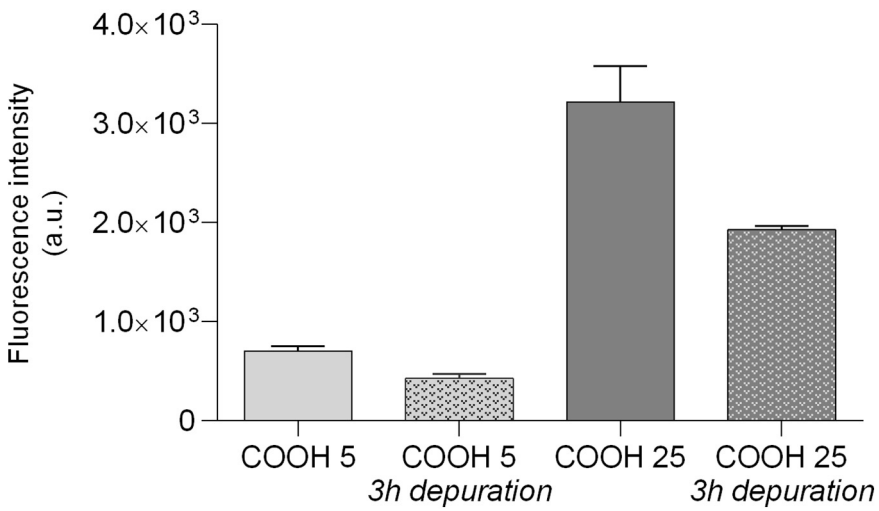

FIGURE 7 | PS-COOH elimination from sea urchin coelomocytes. Fluorescence intensity (arbitrary units, a.u.) of lysates of coelomocytes exposed for 1 h to PS-COOH (5 and 25 μg mL^{-1}) and then left for 3 h in CF. Bars represent mean ± SD (n = 3). Fluorescence intensity is normalized to the auto-fluorescence signal of cells exposed to CF only.

(**Figures 8A,B**). Although no intracellular localization of PS-COOH agglomerates could be followed, results from TEM analysis also indicated substantial differences among the phagocytes exposed to PS NPs and the control group. While untreated cells showed an elongated conformation and high cytoplasmic-to-nuclear ratio, cells exposed to PS-COOH displayed a narrowed structure, slightly damaged cell membranes and filopodia, low cytoplasmic-to-nuclear ratio as well as the presence of foreign material (indicated by the red arrows) (**Figure 9**). As shown in **Figure 9B**, the nucleus

of treated coelomocytes appeared abnormal resembling early apoptosis. However, we cannot disregard that chromatin could have exhibited this conformation due to the orientation of the ultrathin section. Therefore, SEM and TEM analyses of the phagocyte ultrastructure showed that PS NPs were able to affect cell morphology upon short-term acute exposure.

DISCUSSION

The Composition of CF Drives PS NP Behavior

Upon suspension in alkaline and high ionic strength medium, such as seawater, PS NPs are prone both to hetero-agglomeration (i.e., between non-homologous particles) and homo-agglomeration (i.e., among NPs themselves), the latter process driven by high pH (8.0) and ionic composition of the seawater itself (Praetorius et al., 2020). Such behavior is typically more pronounced for anionic PS NPs (i.e., negatively charged PS-COOH) than cationic ones (i.e., positively charged PS-NH_2) (Corsi et al., 2020 and references within), although it still occurs with the formation of agglomerates of PS-NH_2 with the increase in time of exposure (Varó et al., 2019; Eliso et al., 2020) and decrease in temperature of the media (Bergami et al., 2019). The observed agglomeration of PS NPs in sea urchin CF can be thus ascribed to osmolarity and ion composition of the CF, which is in balance with the surrounding seawater, since sea urchins are considered osmoconformers, although some sea urchin species can sustain positive gradients for the most relevant ions (Mg^{2+}, Ca^{2+}, and K^{+}) in case of reduced salinity (Freire et al., 2011; Santos et al., 2013). Moreover, sea urchin CF contains a wide array of biomolecules, produced by the circulating coelomocytes and having key immune functions (Dheilly et al., 2013; Grassi et al., 2019), which are able to adhere on PS NP surface (protein-corona) (Freire et al., 2011; Marques-Santos et al., 2018; Fočak et al., 2019). Our previous findings showed that a highly abundant protein in sea urchin CF, the TPP, tightly bound onto PS NPs surface (hard corona) and provided a new colloidal behavior to PS NPs regardless of their surface charges. Other proteins found adsorbed onto PS NPs in *P. lividus* CF included flotillins, guanine nucleotide-binding proteins and cytoskeletal proteins (Grassi et al., 2019). The observed changes in the absolute surface charges upon incubation in CF of both NPs and furthermore the full neutralization of positive ones of PS-NH_2 determined by EM analysis provide evidence of surface adhesion of biomolecules present in the CF. This is in agreement with our previous findings in which we reported significant changes in PS NP surface charges once suspended in environmental (i.e., sea water) and biological milieux (internal fluids) (Corsi et al., 2020 and references within). However, although still in the nanoscale range, a variability in PS NP agglomerate sizes in CF suspension between the present study (∼300–600 nm) and past investigations (Marques-Santos et al., 2018; Grassi et al., 2019) has been observed and probably related to changes in CF composition in wild caught specimens. While ion composition of sea urchin perivisceral CF can slightly differ from that of external seawater (Freire et al., 2011; Santos et al., 2013), biomolecules secreted by the circulating coelomocytes and microbes inhabiting the fluid, undergo geographical and seasonal fluctuations also as a consequence of their role in several physiological functions including immune defense (Matranga et al., 2005; Branco et al., 2014). Changes in selected ion composition (Na^{+}, other cations and Cl^{-}) have been already documented in sea urchin CF as an adaptive strategy of intertidal species to counteract variations toward external environmental conditions, such as for instance environmental changes in seawater osmolarity (Freire et al., 2011; Fočak et al., 2019). Moreover, a significant increase in the concentration of specific proteins of sea urchin CF (i.e., the toposome, also known as major yolk protein and other molecules) has been reported during the reproductive cycle both in female and male specimens (Ura et al., 2017). Therefore, sea urchin adaptive responses to environmental and physiological changes are reflected by the whole CF composition and thus changes in PS NPs behavior are likely to occur in wild specimens under natural exposure scenarios, potentially affecting NP-induced biological outcomes. A more in-depth characterization of such realistic exposure scenarios is thus required in order to shed light on PS NPs behavior and fate once internalized and distributed in biological fluids of exposed species.

PS NPs Uptake and Clearance

PS-COOH internalization was observed in sea urchin phagocytes, in line with our previous results obtained for cationic PS-NH_2 (Marques-Santos et al., 2018). Phagocytes constitute the largest coelomocyte sub-population (≈80–90%) and play a significant role in sea urchin innate immune response, being actively involved in phagocytosis and encapsulation of foreign particles and microorganisms, wound repair and vesicular transport, as well as the release of humoral components (Smith, 2010; Pinsino and Matranga, 2015). In the Antarctic sea urchin *Sterechinus neumayeri*, the up-regulation of genes associated with antimicrobial peptides was reported in coelomocytes exposed *in vitro* to PS-COOH at 1 and 5 $\mu g\ mL^{-1}$ (Bergami et al., 2019), showing that humoral factors can be involved in PS NP recognition and internalization in sea urchin coelomocytes. Being recognized as a first line of defense in all living beings, phagocytosis represents a consistent response toward a large variety of external stimuli including nanoscale particles uptake and clearance (Smith et al., 2018). Confocal images confirmed the localization of fluorescently labeled PS-COOH agglomerates not only inside the lysosomes of phagocytic cells but also close to their cell membranes where they could stimulate an inflammatory response. The analyses of the phagocyte ultrastructure (through SEM and TEM) showed that PS-COOH were able to affect cell morphology, with impairments in cell membrane and filopodia. Moreover, a higher degree of cell compartmentalization (i.e., higher number of vesicles) could be observed compared to the untreated coelomocytes in the control group. PS NPs are known to act as destabilizers of cell membrane and sub-cellular compartments (Rossi et al., 2014), causing membrane disruption and damage with consequences on cell protective functions. NPs can be internalized by the cells through different pathways, transported and accumulated in the lysosomes but only PS-NH_2 seemed to be able to strongly interact with

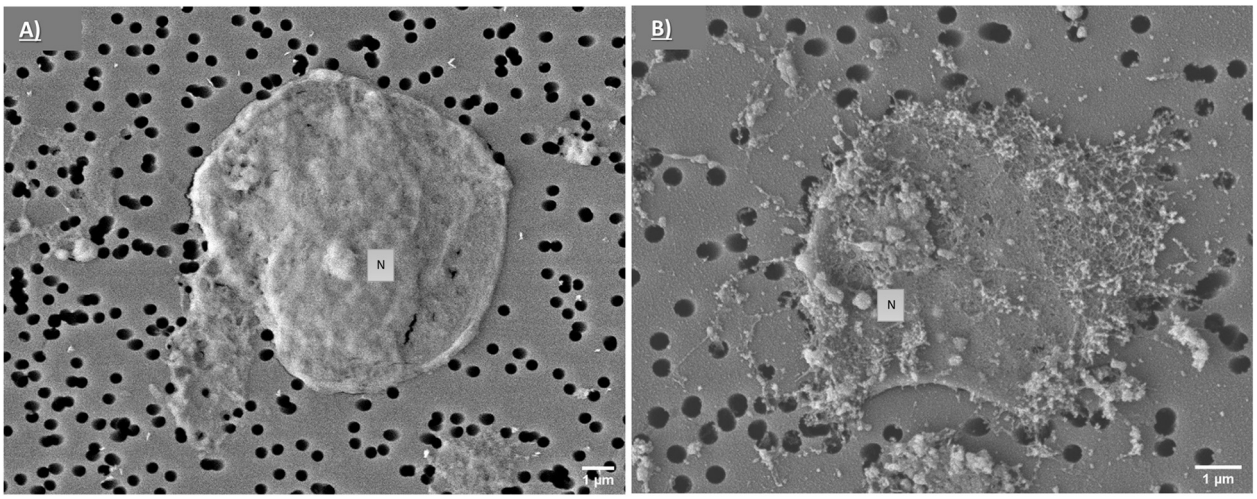

FIGURE 8 | SEM analysis of phagocytes. Representative SEM images of control phagocytes (exposed to CF only) **(A)** and after exposure to PS-COOH at 25 µg mL^{-1} **(B)**. SEM images acquired using a SEM JSM-6700F coupled to LEI detector. Scale bars: 1 µm.

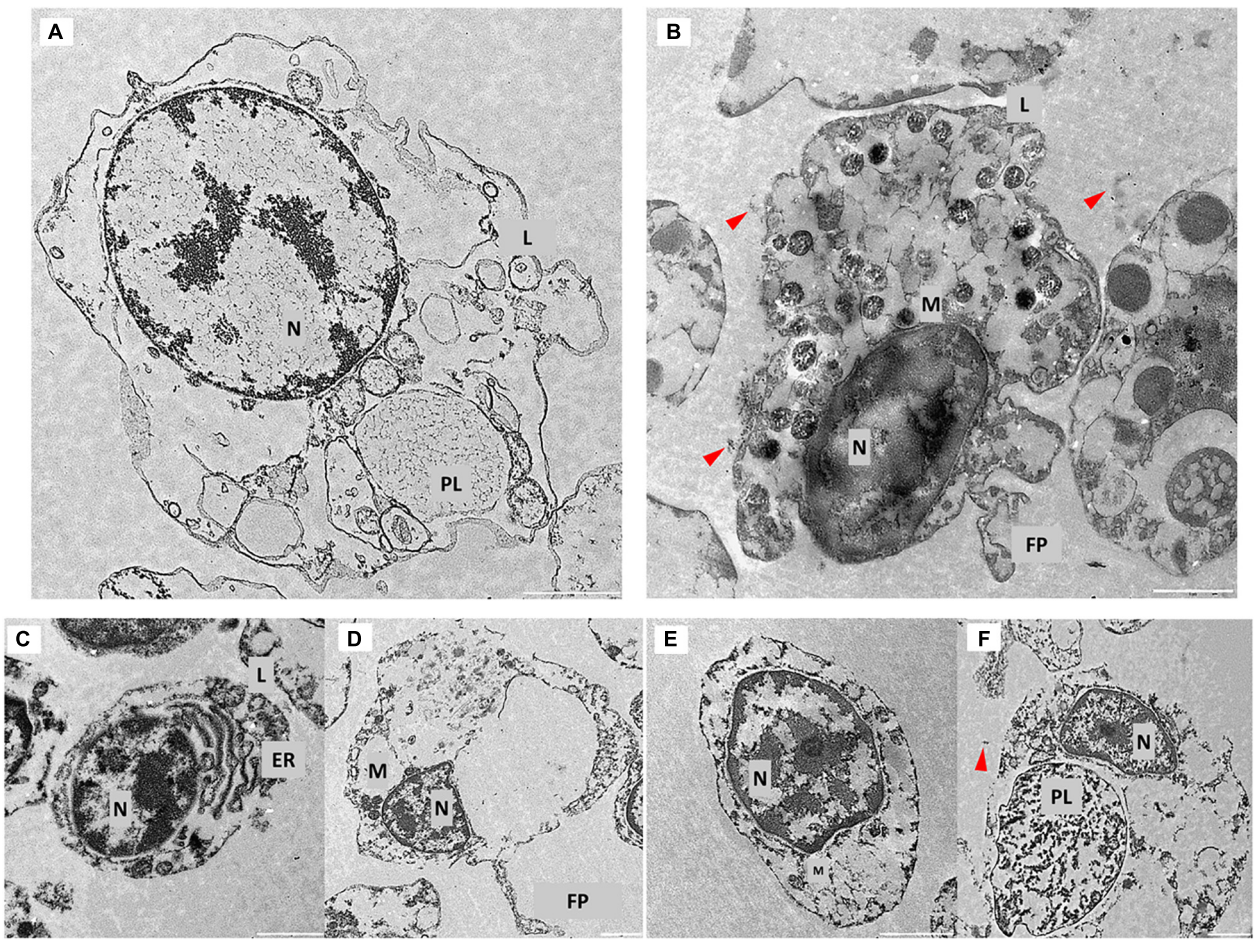

FIGURE 9 | TEM analysis of phagocytes. Representative TEM images of control phagocytes **(A,C,D)** and after exposure to PS-COOH at 25 µg mL^{-1} **(B,E,F)**. Foreign material around cell surface and membrane damage is shown (red arrows). N, nucleus; M, mitochondria; PL, phago-lysosome; L, lysosome; FP, filopodia; ER, endoplasmic reticulum. TEM images were recorded using a LEO 912AB microscope. Scale bars: 1 µm.

biological membranes (Wang et al., 2013a,b). Among these different pathways, phagocytosis is a cellular phenomenon bounded by biophysical constraints and therefore influenced by the concentration as well as the size of the foreign materials (Jaumouillé and Waterman, 2020). A fast internalization (within 1 h of exposure) of PS NPs of similar size (50 nm) has been reported in mussel granulocytes, which share a similar active role in phagocytosis as sea urchin phagocytes (Sendra et al., 2020). A higher ratio of granulocytes/basophilic hyalinocytes was found in their haemolymph upon short-term exposure to PS NPs (50 nm), thus indicative of an intensified immune response (Cole et al., 2020). Phagocytic cells clearly represent a target of PS NPs, whose internalization could trigger the innate immune response of marine invertebrate species and raises concern toward chronic exposure scenarios as those most likely occurring in natural environments. Any breakdown in the response of those cells could result in an impaired ability of marine invertebrates to counteract other toxicities (i.e., exposure to physical, chemical and biological stressors) (Smith et al., 2018). In addition, harmful effects could arise by what PS NPs carry onto their surface, such as for instance contaminants already present in the aquatic environment (e.g., heavy metals, pesticides, hydrocarbons, and pharmaceuticals). As a result, PS NPs could act as vectors of other contaminants and enhance their cellular uptake and accumulation in selected organs (i.e., Trojan horse effect) (Trevisan et al., 2020; Zhang and Xu, 2020).

PS NP Effects on *P. lividus* Immune Response

The immune response exerted by sea urchin coelomocytes differed according to PS NP surface charge. Cell viability did not significantly change upon exposure to PS-COOH compared to the control group, while it was significantly reduced in coelomocytes exposed to PS-NH_2 (25 $\mu g\ mL^{-1}$), in agreement with our previous findings (Marques-Santos et al., 2018). Lysosomal membrane stability was significantly affected only at the highest PS-COOH concentration (25 $\mu g\ mL^{-1}$), but the damage resulted still lower compared to the one caused by PS-NH_2 (25 $\mu g\ mL^{-1}$). Such results are in agreement with our previous findings in which a significant concentration- and time-dependent decrease in lysosomal membrane stability and apoptotic-like nuclear alterations were found in sea urchin phagocytes upon exposure to PS-NH_2 (10 and 25 $\mu g\ mL^{-1}$) (Marques-Santos et al., 2018). A disruption in phagocytosis activity in sea urchin coelomocytes following exposure to PS NPs was observed, in agreement with our previous results on Antarctic sea urchin *Sterechinus neumayeri* (Bergami et al., 2019). Here, the decrease in PC of yeast cells was concentration-dependent in response to PS-COOH (5 and 25 $\mu g\ mL^{-1}$) and a similar effect provoked by PS-COOH and PS-NH_2 at the highest concentration tested was found. Such results can be associated with the active and quick PS NP internalization by sea urchin phagocytes, which limited their ability to respond to further foreign agents and/or pathogens, such as in this case the yeast. However, the significant decrease in PI in response to PS-NH_2 exposure only, compared to the other groups exposed to PS-COOH, suggests that positively charged PS NPs led to a more prominent immunotoxicity, with a reduced activity even among the phagocytes actively internalizing the yeast cells. Alterations in immunological parameters, such as a decrease in PC and an increase in lysozyme activity, have been also reported in mussel haemocytes exposed to PS-NH_2 (50 nm) up to 50 $\mu g\ mL^{-1}$ (Canesi et al., 2015). Bare PS NPs of different sizes (50 nm, 100 nm, 1 μm) have been found to trigger apoptosis and alter PC in mussel haemocytes, *in vitro* exposed (3 h) to similar concentrations (10 mg L^{-1}) (Sendra et al., 2019). In addition, PS NPs suspended in mussel haemolymph acquired a Z-potential approximately of −8.6 −9.6 mV, similar to the one reported for both PS-NPs in this study.

To date, the immunotoxicity of negatively charged PS-COOH in marine invertebrates remains largely unexplored. Our first contribution on the Antarctic sea urchin *S. neumayeri* investigated the effects of PS-COOH and PS-NH_2 (1 and 5 $\mu g\ mL^{-1}$) in coelomocytes through *in vitro* short-term exposure (Bergami et al., 2019). PS-COOH exposure caused a stronger modulation of genes involved in apoptosis and oxidative stress than PS-NH_2, suggesting that PS NP surface charge was the key parameter responsible for toxicity, with cells able to counteract the stress caused by PS-COOH rather than by PS-NH_2 (Bergami et al., 2019). Interestingly, a similar protein corona composition was shared by PS-COOH and PS-NH_2 regardless of their different surface charges (Grassi et al., 2019), nevertheless they were still able to cause a different immune response, with PS-NH_2 being more toxic than PS-COOH. In particular, in our study, both PS NPs affected the PC, however, only PS-NH_2 led to a significant impact on the quality of the phagocytes in terms of PI and on the destabilization of lysosomal membranes. According to Duan and Li (2013), positively charged NPs internalized by the cells could escape from lysosomes after a physical breakdown with an increased influx of chloride ions to counteract their positive charges. Conversely, negatively or un-charged NPs tended to co-localize within lysosomes. Once inside the lysosomes, PS-NH_2 appeared to re-acquire the original positive surface charge due to protein degradation by lysosomal enzymes and loss of the bio-corona. This results in a strong lysosomal dysfunction due to interactions with positive charges according to the proton sponge hypothesis (Nel et al., 2009; Wang et al., 2013a, 2018). This theory may explain why PS-COOH and PS-NH_2 exerted different effects on sea urchin coelomocytes, although they exhibited similar surface charges and protein corona composition in the CF (Grassi et al., 2019). In addition, the smaller average size of PS-NH_2 agglomerates in CF compared to the one of PS-COOH (of ∼330 nm and ∼600 nm, respectively) could play a significant role in particle fate and behavior toward plasma membrane and those of internal organelles as lysosomes.

Our findings support the hypothesis that sea urchin immune cells could be a target of PS NPs and that their surface charge acts as the main driver of potential harmful effects. The efficiency of the sea urchin immune system to counteract the PS-COOH exposure compared to PS-NH_2 is shown and seems to limit any potential risk related to environmental exposure scenarios at relevant concentrations. Predicted environmental concentrations for PS NPs are in the range of 1 pg L^{-1} – 10 $\mu g\ L^{-1}$, far

lower than those tested in the present study (Al-Sid-Cheikh et al., 2018, 2020). However, current projections of global mismanaged plastic waste generation to the next 40 years coupled to ongoing weathering processes and fragmentation, suggest far more critical exposure scenarios in certain marine areas probably not far from the one used in the present study (5–25 $\mu g\ mL^{-1}$) (Lebreton and Andrady, 2019). Plastic accumulation is expected to further intensify in the Mediterranean Sea, recently classified as a hotspot for plastic pollution for both micro- and nanoplastics due local discharges, low dilution and water circulation (Cózar et al., 2015; Suaria et al., 2016; Cincinelli et al., 2019). Recent studies identify in marine sediments the potential reservoir of smaller plastics such as nanoplastics, posing marine benthic species at risk of exposure (Llorca et al., 2020). PS-COOH are more likely to resemble the naturally occurring negatively surface charged nanoplastics, which may end up in marine coastal waters from primary and secondary sources (Hernandez et al., 2017; Tian et al., 2019). As a result of weathering, most plastics break down into nanoscale plastic fragments, as demonstrated for large PS-based products (Lambert and Wagner, 2016) and they acquire negative surface charges (Fotopoulou and Karapanagioti, 2012; Andrady, 2017). Therefore, the exposure levels for benthic organisms, particularly those inhabiting Mediterranean shallow coastal areas, are likely to exceed toxicity-thresholds.

Overall, these findings improve our understanding on the interplay between negatively charged PS NPs, as a proxy for naturally occurring nanoplastics, and *P. lividus* immune system. A fast uptake by phagocytes and sequestration into lysosomal compartments has been demonstrated, with associated low acute toxicity in comparison with their positively charged counterparts. Although experimental conditions considered in the present study reflect acute and probably unrealistic exposure scenarios, they may be representative of local worst-case scenarios, such as the ones occurring in Mediterranean shallow waters. As a matter of fact, under conditions of nanoplastic accumulation in marine coastal sediments and upon acting as vectors of other pollutants, PS-COOH could still pose a threat to the Mediterranean benthic communities.

DATA AVAILABILITY STATEMENT

The raw data supporting the conclusions of this article will be made available by the authors, without undue reservation.

AUTHOR CONTRIBUTIONS

CM: data curation, formal analysis, investigation, methodology, visualization, and writing – original draft. EB: data curation, formal analysis, methodology, writing – review and editing. GL: data curation, formal analysis, and methodology. AP: funding acquisition, writing – review and editing. IC: conceptualization, supervision, writing – review and editing, resources, and funding acquisition. All authors contributed to the article and approved the submitted version.

FUNDING

CM was supported by a Ph.D. fellowship co-funded by University of Siena and Stazione Zoologica Anton Dohrn.

ACKNOWLEDGMENTS

The authors thank all staff of the Advanced Microscopy Center (RIMAR department, Stazione Zoologica Anton Dohrn) for the invaluable support for SEM and TEM analyses. DLS analysis was performed at the Centro Ricerca Energia e Ambiente (CREA, University of Siena, Italy: www.crea.unisi.it), with the support of Dr. Marianna Uva.

SUPPLEMENTARY MATERIAL

The Supplementary Material for this article can be found online at: https://www.frontiersin.org/articles/10.3389/fmars.2021.647394/full#supplementary-material

REFERENCES

Abidli, S., Antunes, J. C., Ferreira, J. L., Lahbib, Y., Sobral, P., and Trigui El Menif, N. (2018). Microplastics in sediments from the littoral zone of the north Tunisian coast (Mediterranean Sea). *Estuar. Coast. Shelf Sci.* 205, 1–9. doi: 10.1016/j.ecss.2018.03.006

Abidli, S., Lahbib, Y., and Trigui El Menif, N. (2019). Microplastics in commercial molluscs from the lagoon of Bizerte (Northern Tunisia). *Mar. Pollut. Bull.* 142, 243–252. doi: 10.1016/j.marpolbul.2019.03.048

Alijagic, A., Gaglio, D., Napodano, E., Russo, R., Costa, C., Benada, O., et al. (2020). Titanium dioxide nanoparticles temporarily influence the sea urchin immunological state suppressing inflammatory-relate gene transcription and boosting antioxidant metabolic activity. *J. Hazard. Mater.* 384:121389. doi: 10.1016/j.jhazmat.2019.121389

Alomar, C., Estarellas, F., and Deudero, S. (2016). Microplastics in the Mediterranean Sea: deposition in coastal shallow sediments, spatial variation and preferential grain size. *Mar. Environ. Res.* 115, 1–10. doi: 10.1016/j.marenvres.2016.01.005

Al-Sid-Cheikh, M., Rowland, S. J., Kaegi, R., Henry, T. B., Cormier, M.-A., and Thompson, R. C. (2020). Synthesis of ^{14}C-labelled polystyrene nanoplastics for environmental studies. *Commun. Mater.* 1:97. doi: 10.1038/s43246-020-00097-9

Al-Sid-Cheikh, M., Rowland, S. J., Stevenson, K., Rouleau, C., Henry, T. B., and Thompson, R. C. (2018). Uptake, whole-body distribution, and depuration of nanoplastics by the scallop *Pecten maximus* at environmentally realistic concentrations. *Environ. Sci. Technol.* 52, 14480–14486. doi: 10.1021/acs.est.8b05266

Andrady, A. L. (2017). The plastic in microplastics: a review. *Mar. Pollut. Bull.* 119, 12–22. doi: 10.1016/j.marpolbul.2017.01.082

Angiolillo, M., di Lorenzo, B., Farcomeni, A., Bo, M., Bavestrello, G., Santangelo, G., et al. (2015). Distribution and assessment of marine debris in the deep Tyrrhenian Sea (NW Mediterranean Sea. Italy). *Mar. Pollut. Bull.* 92, 149–159. doi: 10.1016/j.marpolbul.2014.12.044

Avio, C. G., Cardelli, L. R., Gorbi, S., Pellegrini, D., and Regoli, F. (2017). Microplastics pollution after the removal of the Costa Concordia wreck: first evidences from a biomonitoring case study. *Environ. Pollut.* 227, 207–214. doi: 10.1016/j.envpol.2017.04.066

Barnes, D., Verling, E., Crook, A., Davidson, I., and O'Mahoney, M. (2002). Local population disappearance follows (20 yr after) cycle collapse in a pivotal ecological species. *Mar. Ecol. Prog. Ser.* 226, 311–313. doi: 10.3354/meps226311

Bergami, E., Bocci, E., Vannuccini, M. L., Monopoli, M., Salvati, A., Dawson, K. A., et al. (2016). Nano-sized polystyrene affects feeding, behavior and physiology of brine shrimp *Artemia franciscana* larvae. *Ecotoxicol. Environ. Saf.* 123, 18–25. doi: 10.1016/j.ecoenv.2015.09.021

Bergami, E., Krupinski Emerenciano, A., González-Aravena, M., Cárdenas, C. A., Hernández, P., Silva, J. R. M. C., et al. (2019). Polystyrene nanoparticles affect the innate immune system of the Antarctic sea urchin *Sterechinus neumayeri*. *Polar Biol.* 42, 743–757. doi: 10.1007/s00300-019-02468-6

Bergami, E., Pugnalini, S., Vannuccini, M. L., Manfra, L., Faleri, C., Savorelli, F., et al. (2017). Long-term toxicity of surface-charged polystyrene nanoplastics to marine planktonic species *Dunaliella tertiolecta* and *Artemia franciscana*. *Aquat. Toxicol.* 189, 159–169. doi: 10.1016/j.aquatox.2017.06.008

Borges, J., Porto-Neto, L., Mangiaterra, M., Jensch-Junior, B., and da Silva, J. (2002). Phagocytosis *in vitro* and *in vivo* in the Antarctic sea urchin *Sterechinus neumayeri* at 0°C. *Polar Biol.* 25, 891–897. doi: 10.1007/s00300-002-0431-6

Boudouresque, C. F., and Verlaque, M. (2020). "Paracentrotus lividus," in *Developments in Aquaculture and Fisheries Science*, ed. J. M. Lawrence (Amsterdam: Elsevier), 447–485. doi: 10.1016/B978-0-12-819570-3.00026-3

Branco, P., Figueiredo, D., and da Silva, J. R. M. C. (2014). New insights into innate immune system of sea urchin: coelomocytes as biosensors for environmental stress. *Crit. Rev.* 7, 1–7.

Branco, P. C., Borges, J. C. S., Santos, M. F., Jensch Junior, B. E., and da Silva, J. R. M. C. (2013). The impact of rising sea temperature on innate immune parameters in the tropical subtidal sea urchin Lytechinus variegatus and the intertidal sea urchin Echinometra lucunter. *Mar. Environ. Res.* 92, 95–101. doi: 10.1016/j.marenvres.2013.09.005

Canesi, L., Ciacci, C., Bergami, E., Monopoli, M. P., Dawson, K. A., Papa, S., et al. (2015). Evidence for immunomodulation and apoptotic processes induced by cationic polystyrene nanoparticles in the hemocytes of the marine bivalve Mytilus. *Mar. Environ. Res.* 111, 34–40. doi: 10.1016/j.marenvres.2015.06.008

Canesi, L., Ciacci, C., Fabbri, R., Balbi, T., Salis, A., Damonte, G., et al. (2016). Interactions of cationic polystyrene nanoparticles with marine bivalve hemocytes in a physiological environment: role of soluble hemolymph proteins. *Environ. Res.* 150, 73–81. doi: 10.1016/j.envres.2016.05.045

Canesi, L., and Corsi, I. (2016). Effects of nanomaterials on marine invertebrates. *Sci. Total Environ.* 565, 933–940. doi: 10.1016/j.scitotenv.2016.01.085

Castellano, I., Migliaccio, O., Ferraro, G., Maffioli, E., Marasco, D., Merlino, A., et al. (2018). Biotic and environmental stress induces nitration and changes in structure and function of the sea urchin major yolk protein toposome. *Sci. Rep.* 8:4610. doi: 10.1038/s41598-018-22861-1

Catarino, A. I., Frutos, A., and Henry, T. B. (2019). Use of fluorescent-labelled nanoplastics (NPs) to demonstrate NP absorption is inconclusive without adequate controls. *Sci. Total Environ.* 670, 915–920. doi: 10.1016/j.scitotenv.2019.03.194

Cincinelli, A., Martellini, T., Guerranti, C., Scopetani, C., Chelazzi, D., and Giarrizzo, T. (2019). A potpourri of microplastics in the sea surface and water column of the Mediterranean Sea. *TrAC Trends Anal. Chem.* 110, 321–326. doi: 10.1016/j.trac.2018.10.026

Cole, M., Liddle, C., Consolandi, G., Drago, C., Hird, C., Lindeque, P. K., et al. (2020). Microplastics, microfibres and nanoplastics cause variable sub-lethal responses in mussels (*Mytilus* spp.). *Mar. Pollut. Bull.* 160:111552. doi: 10.1016/j.marpolbul.2020.111552

Compa, M., Alomar, C., Wilcox, C., van Sebille, E., Lebreton, L., Hardesty, B. D., et al. (2019). Risk assessment of plastic pollution on marine diversity in the Mediterranean Sea. *Sci. Total Environ.* 678, 188–196. doi: 10.1016/j.scitotenv.2019.04.355

Consoli, P., Falautano, M., Sinopoli, M., Perzia, P., Canese, S., Esposito, V., et al. (2018). Composition and abundance of benthic marine litter in a coastal area of the central Mediterranean Sea. *Mar. Pollut. Bull.* 136, 243–247. doi: 10.1016/j.marpolbul.2018.09.033

Corsi, I., Bergami, E., and Grassi, G. (2020). Behaviour and bio-interactions of anthropogenic particles in marine environment for a more realistic ecological risk assessment. *Front. Environ. Sci.* 8:60. doi: 10.3389/fenvs.2020.00060

Courtene-Jones, W., Quinn, B., Gary, S. F., Mogg, A. O. M., and Narayanaswamy, B. E. (2017). Microplastic pollution identified in deep-sea water and ingested by benthic invertebrates in the Rockall Trough. North Atlantic Ocean. *Environ. Pollut.* 231, 271–280. doi: 10.1016/j.envpol.2017.08.026

Cózar, A., Sanz-Martín, M., Martí, E., González-Gordillo, J. I., Ubeda, B., Gálvez, J. Á, et al. (2015). Plastic Accumulation in the Mediterranean Sea. *PLoS One* 10:e0121762. doi: 10.1371/journal.pone.0121762

Davies, I. M., Gubbins, M., Hylland, K., Maes, T., Martínez-Gómez, C., Giltrap, M., et al. (2012). "Technical annex: assessment criteria for biological effects measurements, 209-212," in *Integrated Monitoring of Chemicals and Their Effects. ICES Cooperative Research Report: 315*, eds I. M. Davies and A. D. Vethaak (Copenhagen: ICES).

Della Torre, C., Bergami, E., Salvati, A., Faleri, C., Cirino, P., Dawson, K. A., et al. (2014). Accumulation and embryotoxicity of polystyrene nanoparticles at early stage of development of sea urchin embryos *Paracentrotus lividus*. *Environ. Sci. Technol.* 48, 12302–12311. doi: 10.1021/es502569w

Dheilly, N. M., Raftos, D. A., Haynes, P. A., Smith, L. C., and Nair, S. V. (2013).). Shotgun proteomics of coelomic fluid from the purple sea urchin, Strongylocentrotus purpuratus. *Dev. Comp. Immunol.* 40, 35–50. doi: 10.1016/j.dci.2013.01.007

Duan, X., and Li, Y. (2013). Physicochemical characteristics of nanoparticles affect circulation, biodistribution, cellular internalization, and trafficking. *Small* 9, 1521–1532. doi: 10.1002/smll.201201390

Eliso, M. C., Bergami, E., Manfra, L., Spagnuolo, A., and Corsi, I. (2020). Toxicity of nanoplastics during the embryogenesis of the ascidian *Ciona robusta* (Phylum Chordata). *Nanotoxicology* 14, 1415–1431. doi: 10.1080/17435390.2020.1838650

Falugi, C., Aluigi, M. G., Chiantore, M. C., Privitera, D., Ramoino, P., Gatti, M. A., et al. (2012). Toxicity of metal oxide nanoparticles in immune cells of the sea urchin. *Mar. Environ. Res.* 76, 114–121. doi: 10.1016/j.marenvres.2011.10.003

Feng, L. J., Li, J. W., Xu, E. G., Sun, X. D., Zhu, F. P., Ding, Z., et al. (2019). Short-term exposure to positively charged polystyrene nanoparticles causes oxidative stress and membrane destruction in cyanobacteria. *Environ. Sci. Nano* 6, 3072–3079. doi: 10.1039/C9EN00807A

Feng, Z., Wang, R., Zhang, T., Wang, J., Huang, W., Li, J., et al. (2020). Microplastics in specific tissues of wild sea urchins along the coastal areas of northern China. *Sci. Total Environ.* 728:138660. doi: 10.1016/j.scitotenv.2020.138660

Fočak, M., Džafiæ, S., and Suljeviæ, D. (2019). Electrolites and heavy metals in coelomic fluid of sea urchin, arbacia lixula from adriatic sea: biochemical approach to ecotoxicological study. *Naše More* 66, 51–56. doi: 10.17818/NM/2019/2.1

Fotopoulou, K. N., and Karapanagioti, H. K. (2012). Surface properties of beached plastic pellets. *Mar. Environ. Res.* 81, 70–77. doi: 10.1016/j.marenvres.2012.08.010

Freire, C. A., Santos, I. A., and Vidolin, D. (2011). Osmolality and ions of the perivisceral coelomic fluid of the intertidal sea urchin Echinometra lucunter (*Echinodermata*: *Echinoidea*) upon salinity and ionic challenges. *Zoologia* 28, 479–487. doi: 10.1590/S1984-46702011000400009

Gigault, J., Pedrono, B., Maxit, B., and Ter Halle, A. (2016). Marine plastic litter: the unanalyzed nano-fraction. *Environ. Sci. Nano* 3, 346–350. doi: 10.1039/C6EN00008H

Graham, E. R., and Thompson, J. T. (2009). Deposit- and suspension-feeding sea cucumbers (*Echinodermata*) ingest plastic fragments. *J. Exp. Mar. Biol. Ecol.* 368, 22–29. doi: 10.1016/j.jembe.2008.09.007

Grassi, G., Landi, C., Torre, C. D., Bergami, E., Bini, L., and Corsi, I. (2019). Proteomic profile of the hard corona of charged polystyrene nanoparticles exposed to sea urchin *Paracentrotus lividus* coelomic fluid highlights potential drivers of toxicity. *Environ. Sci. Nano* 6, 2937–2947. doi: 10.1039/C9EN00824A

Hartmann, N. B., Hüffer, T., Thompson, R. C., Hassellöv, M., Verschoor, A., Daugaard, A. E., et al. (2019). Are we speaking the same language? Recommendations for a definition and categorization framework for plastic debris. *Environ. Sci. Technol.* 53, 1039–1047. doi: 10.1021/acs.est.8b05297

Hernandez, E., Nowack, B., and Mitrano, D. M. (2017). Polyester Textiles as a source of microplastics from households: a mechanistic study to understand microfiber release during Washing. *Environ. Sci. Technol.* 51, 7036–7046. doi: 10.1021/acs.est.7b01750

Hewitt, R. E., Chappell, H. F., and Powell, J. J. (2020). Small and dangerous? Potential toxicity mechanisms of common exposure particles and nanoparticles. *Curr. Opin. Toxicol.* 19, 93–98. doi: 10.1016/j.cotox.2020.01.006

ICES (2010). *Report of the ICES\OSPAR Workshop on Lysosomal Stability Data Quality and Interpretation (WKLYS), 13–17 September 2010*. Alessandria: ICES CM2010/ACOM: 61.

Jaumouillé, V., and Waterman, C. M. (2020). Physical constraints and forces involved in phagocytosis. *Front. Immunol.* 11:1097. doi: 10.3389/fimmu.2020.01097

Kane, I. A., Clare, M. A., Miramontes, E., Wogelius, R., Rothwell, J. J., Garreau, P., et al. (2020). Seafloor microplastic hotspots controlled by deep-sea circulation. *Science* 368, 1140–1145. doi: 10.1126/science.aba5899

Lambert, C., Authier, M., Dorémus, G., Laran, S., Panigada, S., Spitz, J., et al. (2020). Setting the scene for Mediterranean litterscape management: the first basin-scale quantification and mapping of floating marine debris. *Environ. Pollut.* 263:114430. doi: 10.1016/j.envpol.2020.114430

Lambert, S., and Wagner, M. (2016). Characterisation of nanoplastics during the degradation of polystyrene. *Chemosphere* 145, 265–268. doi: 10.1016/j.chemosphere.2015.11.078

Lead, J. R., Batley, G. E., Alvarez, P. J. J., Croteau, M.-N., Handy, R. D., McLaughlin, M. J., et al. (2018). Nanomaterials in the environment: behavior, fate, bioavailability, and effects-An updated review: nanomaterials in the environment. *Environ. Toxicol. Chem.* 37, 2029–2063. doi: 10.1002/etc.4147

Lebreton, L., and Andrady, A. (2019). Future scenarios of global plastic waste generation and disposal. *Palgrave Commun.* 5:6. doi: 10.1057/s41599-018-0212-7

Llorca, M., Vega-Herrera, A., Schirinzi, G., Savva, K., Abad, E., and Farré, M. (2020). Screening of suspected micro(nano)plastics in the Ebro Delta (Mediterranean Sea). *J. Hazard. Mater.* 404:124022. doi: 10.1016/j.jhazmat.2020.124022

Lowe, D., Fossato, V., and Depledge, M. (1995). Contaminant-induced lysosomal membrane damage in blood cells of mussels *Mytilus galloprovincialis* from the Venice Lagoon:an in vitro study. *Mar. Ecol. Prog. Ser.* 129, 189–196. doi: 10.3354/meps129189

Lowry, G. V., Gregory, K. B., Apte, S. C., and Lead, J. R. (2012). Transformations of Nanomaterials in the Environment. *Environ. Sci. Technol.* 46, 6893–6899. doi: 10.1021/es300839e

Macias, D., Cózar, A., Garcia-Gorriz, E., González-Fernández, D., and Stips, A. (2019). Surface water circulation develops seasonally changing patterns of floating litter accumulation in the Mediterranean Sea. A modelling approach. *Mar. Pollut. Bull.* 149:110619. doi: 10.1016/j.marpolbul.2019.110619

Macic, V., Mandic, M., Pestoric, B., Gacic, Z., and Paunovic, M. (2017). First assessment of marine litter in shallow south-east Adriatic Sea. *Fresenius Env. Bull.* 26, 4834–4880.

Majeske, A. J., Bayne, C. J., and Smith, L. C. (2013). Aggregation of sea urchin phagocytes is augmented *In Vitro* by lipopolysaccharide. *PLoS One* 8:61419. doi: 10.1371/journal.pone.0061419

Manfra, L., Rotini, A., Bergami, E., Grassi, G., Faleri, C., and Corsi, I. (2017). Comparative ecotoxicity of polystyrene nanoparticles in natural seawater and reconstituted seawater using the rotifer Brachionus plicatilis. *Ecotoxicol. Environ. Saf.* 145, 557–563. doi: 10.1016/j.ecoenv.2017.07.068

Marques-Santos, L. F., Grassi, G., Bergami, E., Faleri, C., Balbi, T., Salis, A., et al. (2018). Cationic polystyrene nanoparticle and the sea urchin immune system: biocorona formation, cell toxicity, and multixenobiotic resistance phenotype. *Nanotoxicology* 12, 847–867. doi: 10.1080/17435390.2018.1482378

Matranga, V., Bonaventura, R., and Di Bella, G. (2002). Hsp70 as a stress marker of sea urchin coelomocytes in short term cultures. *Cell Mol. Biol.* 48, 345–349.

Matranga, V., Pinsino, A., Celi, M., Natoli, A., Bonaventura, R., Schröder, H. C., et al. (2005). "Monitoring chemical and physical stress using sea urchin immune cells," in *Echinodermata Progress in Molecular and Subcellular Biology*, ed. V. Matranga (Berlin: Springer-Verlag), 85–110. doi: 10.1007/3-540-27683-1_5

Mattsson, K., Jocic, S., Doverbratt, I., and Hansson, L.-A. (2018). "Nanoplastics in the aquatic environment," in *Microplastic Contamination in Aquatic Environments*, ed. E. Y. Zeng (Amsterdam: Elsevier), 379–399. doi: 10.1016/B978-0-12-813747-5.00013-8

Migliaccio, O., Pinsino, A., Maffioli, E., Smith, A. M., Agnisola, C., Matranga, V., et al. (2019). Living in future ocean acidification, physiological adaptive responses of the immune system of sea urchins resident at a CO_2 vent system. *Sci. Total Environ.* 672, 938–950. doi: 10.1016/j.scitotenv.2019.04.005

Milito, A., Murano, C., Castellano,I., Romano, G., and Palumbo, A. (2020). Antioxidant and immune response of the sea urchin Paracentrotus lividus to different re-suspension patterns of highly polluted marine sediments. *Mar. Environ. Res.* 160:104978. doi: 10.1016/j.marenvres.2020.104978

Murano, C., Agnisola, C., Caramiello, D., Castellano, I., Casotti, R., Corsi, I., et al. (2020). How sea urchins face microplastics: uptake, tissue distribution and immune system response. *Environ. Pollut.* 264:114685. doi: 10.1016/j.envpol.2020.114685

Nel, A. E., Mädler, L., Velegol, D., Xia, T., Hoek, E. M. V., Somasundaran, P., et al. (2009). Understanding biophysicochemical interactions at the nano–bio interface. *Nat. Mater.* 8, 543–557. doi: 10.1038/nmat2442

Pawley, J. B. (2006). *Fundamental Limits in Confocal Microscopy. Handbook of Biological Confocal Microscopy*, 3rd Edn. New York, NY: Springer Science+ Business Media, LLC.

Pikuda, O., Xu, E. G., Berk, D., and Tufenkji, N. (2019). Toxicity assessments of micro- and nanoplastics can be confounded by preservatives in commercial formulations. *Environ. Sci. Technol. Lett.* 6, 21–25. doi: 10.1021/acs.estlett.8b00614

Pinsino, A., Bergami, E., Della Torre, C., Vannuccini, M. L., Addis, P., Secci, M., et al. (2017). Amino-modified polystyrene nanoparticles affect signalling pathways of the sea urchin (*Paracentrotus lividus)* embryos. *Nanotoxicology* 11, 201–209. doi: 10.1080/17435390.2017.1279360

Pinsino, A., and Matranga, V. (2015). Sea urchin immune cells as sentinels of environmental stress. *Dev. Comp. Immunol.* 49, 198–205. doi: 10.1016/j.dci.2014.11.013

Pinsino, A., Russo, R., Bonaventura, R., Brunelli, A., Marcomini, A., and Matranga, V. (2015). Titanium dioxide nanoparticles stimulate sea urchin immune cell phagocytic activity involving TLR/p38 MAPK-mediated signalling pathway. *Sci. Rep.* 5:14492. doi: 10.1038/srep14492

Plee, T. A., and Pomory, C. M. (2020). Microplastics in sandy environments in the Florida Keys and the panhandle of Florida, and the ingestion by sea cucumbers (*Echinodermata*: *Holothuroidea*) and sand dollars (*Echinodermata*: *Echinoidea*). *Mar. Polluti. Bull.* 158:111437. doi: 10.1016/j.marpolbul.2020.111437

Porter, A., Smith, K. E., and Lewis, C. (2019). The sea urchin *Paracentrotus lividus* as a bioeroder of plastic. *Sci. Total Environ.* 693:133621. doi: 10.1016/j.scitotenv.2019.133621

Praetorius, A., Badetti, E., Brunelli, A., Clavier, A., Gallego-Urrea, J. A., Gondikas, A., et al. (2020). Strategies for determining heteroaggregation attachment efficiencies of engineered nanoparticles in aquatic environments. *Environ. Sci. Nano* 7, 351–367. doi: 10.1039/C9EN01016E

Rossi, G., Barnoud, J., and Monticelli, L. (2014). Polystyrene Nanoparticles Perturb Lipid Membranes. *J. Phys. Chem. Lett.* 5, 241–246. doi: 10.1021/jz402234c

Santos, I. A., Castellano, G. C., and Freire, C. A. (2013). Direct relationship between osmotic and ionic conforming behavior and tissue water regulatory capacity in echinoids. *Comp. Biochem. Physiol. Part A Mol. Integr. Physiol.* 164, 466–476. doi: 10.1016/j.cbpa.2012.12.010

Schirinzi, G. F., Llorca, M., Seró, R., Moyano, E., Barceló, D., Abad, E., et al. (2019). Trace analysis of polystyrene microplastics in natural waters. *Chemosphere* 236:124321. doi: 10.1016/j.chemosphere.2019.07.052

Schür, C., Rist, S., Baun, A., Mayer, P., Hartmann, N. B., and Wagner, M. (2019). When fluorescence is not a particle: the tissue translocation of microplastics in *Daphnia magna* Seems an Artifact. *Environ. Toxicol. Chem.* 38, 1495–1503. doi: 10.1002/etc.4436

Sendra, M., Carrasco-Braganza, M. I., Yeste, P. M., Vila, M., and Blasco, J. (2020). Immunotoxicity of polystyrene nanoplastics in different hemocyte subpopulations of *Mytilus galloprovincialis*. *Sci. Rep.* 10:8637. doi: 10.1038/s41598-020-65596-8

Sendra, M., Saco, A., Yeste, M. P., Romero, A., Novoa, B., and Figueras, A. (2019). Nanoplastics: From tissue accumulation to cell translocation into *Mytilus galloprovincialis* hemocytes. resilience of immune cells exposed to nanoplastics and nanoplastics plus Vibrio splendidus combination. *J. Hazard. Mater.* 388:121788. doi: 10.1016/j.jhazmat.2019.121788

Simon-Sánchez, L., Grelaud, M., Garcia-Orellana, J., and Ziveri, P. (2019). River Deltas as hotspots of microplastic accumulation: the case study of the Ebro River (NW Mediterranean). *Sci. Total Environ.* 687, 1186–1196. doi: 10.1016/j.scitotenv.2019.06.168

Smith, L. C. (2010). Diversification of innate immune genes: lessons from the purple sea urchin. *Dis. Models Mech.* 3, 274–279. doi: 10.1242/dmm.004697

Smith, L. C., Arizza, V., Barela Hudgell, M. A., Barone, G., Bodnar, A. G., Buckley, K. M., et al. (2018). "*Echinodermata*: the complex immune system in echinoderms," in *Advances in Comparative Immunology*, ed. E. L. Cooper (Cham: Springer International Publishing), 409–501. doi: 10.1007/978-3-319-76768-0_13

Smith, L. C., Hawley, T. S., Henson, J. H., Majeske, A. J., Oren, M., and Rosental, B. (2019). "Chapter 15 – methods for collection, handling, and analysis of sea urchin coelomocytes," in *Methods in Cell Biology Echinoderms, Part A.*, eds K. R. Foltz and A. Hamdoun (Academic Press), 357–389. doi: 10.1016/bs.mcb.2018.11.009

Strober, W. (2015). Trypan blue exclusion test of cell viability. *Curr. Protoc. Immunol.* 111, A3.B.1–A3.B.3. doi: 10.1002/0471142735.ima03bs111

Suaria, G., Avio, C. G., Mineo, A., Lattin, G. L., Magaldi, M. G., Belmonte, G., et al. (2016). The mediterranean plastic soup: synthetic polymers in mediterranean surface waters. *Sci. Rep.* 6:37551. doi: 10.1038/srep37551

Tallec, K., Blard, O., González-Fernández, C., Brotons, G., Berchel, M., Soudant, P., et al. (2019). Surface functionalization determines behavior of nanoplastic solutions in model aquatic environments. *Chemosphere* 225, 639–646. doi: 10.1016/j.chemosphere.2019.03.077

Taylor, M. L., Gwinnett, C., Robinson, L. F., and Woodall, L. C. (2016). Plastic microfibre ingestion by deep-sea organisms. *Sci. Rep.* 6:33997. doi: 10.1038/srep33997

Tian, L., Chen, Q., Jiang, W., Wang, L., Xie, H., Kalogerakis, N., et al. (2019). A carbon-14 radiotracer-based study on the phototransformation of polystyrene nanoplastics in water versus in air. *Environ. Sci. Nano* 6, 2907–2917. doi: 10.1039/C9EN00662A

Trevisan, R., Uzochukwu, D., and Di Giulio, R. (2020). PAH sorption to nanoplastics and the trojan horse effect as drivers of Mitochondrial Toxicity and PAH Localization in Zebrafish. *Front. Environ. Sci.* 8:78. doi: 10.3389/fenvs.2020.00078

Ura, K., Wang, H., Hori, T., Aizawa, S., Tsue, S., Satoh, M., et al. (2017). The reproductive cycle and transcription-level changes in the major yolk protein of wild northern sea urchin. *Aquacult. Sci.* 65, 231–237.

Varó, I., Perini, A., Torreblanca, A., Garcia, Y., Bergami, E., Vannuccini, M. L., et al. (2019). Time-dependent effects of polystyrene nanoparticles in brine shrimp *Artemia franciscana* at physiological, biochemical and molecular levels. *Sci. Total Environ.* 675, 570–580. doi: 10.1016/j.scitotenv.2019.04.157

Vered, G., Kaplan, A., Avisar, D., and Shenkar, N. (2019). Using solitary ascidians to assess microplastic and phthalate plasticizers pollution among marine biota: a case study of the Eastern Mediterranean and Red Sea. *Mar. Pollut. Bull.* 138, 618–625. doi: 10.1016/j.marpolbul.2018.12.013

Wang, F., Bexiga, M. G., Anguissola, S., Boya, P., Simpson, J. C., Salvati, A., et al. (2013a). Time resolved study of cell death mechanisms induced by amine-modified polystyrene nanoparticles. *Nanoscale* 5:10868. doi: 10.1039/c3nr03249c

Wang, F., Yu, L., Monopoli, M. P., Sandin, P., Mahon, E., Salvati, A., et al. (2013b). The biomolecular corona is retained during nanoparticle uptake and protects the cells from the damage induced by cationic nanoparticles until degraded in the lysosomes. *Nanomedicine*9, 1159–1168. doi: 10.1016/j.nano.2013.04.010

Wang, F., Salvati, A., and Boya, P. (2018). Lysosome-dependent cell death and deregulated autophagy induced by amine-modified polystyrene nanoparticles. *Open Biol.* 8:170271. doi: 10.1098/rsob.170271

Zhang, M., and Xu, L. (2020). Transport of micro- and nanoplastics in the environment: trojan-horse effect for organic contaminants. *Crit. Rev. Environ. Sci. Technol.* 12, 1–37. doi: 10.1080/10643389.2020.1845531

Conflict of Interest: The authors declare that the research was conducted in the absence of any commercial or financial relationships that could be construed as a potential conflict of interest.